Impact Force Identification of CFRP Structures Using Experimental Transfer Matrices

S. Atobe[1], H. Fukunaga[1] and N. Hu[2]

Abstract: This paper presents a method for identifying the location and force history of an impact force acting on CFRP structures such as laminated plates and stiffened panels. The identification method is an experimental one without using any analytical model of the structure. Here, experimental transfer matrices, which relate the impact force to the corresponding responses of PZT sensors, are used to identify the impact force. The transfer matrices are preliminarily constructed from the measured data obtained by impact tests with an impulse hammer. To identify the impact location, the arrival times of the flexural waves to the PZT sensors are used, and an analog band-pass filter is used to obtain waves with a specified frequency. The wave velocity is determined experimentally from impact test results. The present method is verified experimentally by performing impact force identification of CFRP laminated plates and CFRP stiffened panels. The results reveal that the location and force history of the impact force can be identified accurately and rapidly using the present method.

Keywords: Identification, impact location, force history, CFRP structures.

1 Introduction

In recent years, structural health monitoring (SHM) is receiving wide attention as a promising technique for ensuring the safety and improving the maintainability of aerospace structures [Staszewski, Boller and Tomlinson (2004)]. Generally, a SHM system is for automatically monitoring the damage and assessing the structural integrity in real time by using the measured responses obtained from a built-in sensor network. In the case of composite structures, which are now extensively applied to the primary structural components of aircrafts, a major issue is the monitoring of impact damages that are induced by foreign object impacts or dynamic contacts [Hu (1997); Sekine and Hu (1998); Hu, Sekine, Fukunaga and Yao (1999);

---

[1] Tohoku University, Sendai, Japan.
[2] Chiba University, Chiba, Japan.

Li, Hu, Yin, Sekine and Fukunaga (2002); Li, Hu, Cheng, Fukunaga and Sekine (2002); Hu, Zemba, Okabe, Yan, Fukunaga and Elmarakbi (2008)]. Among the various types of SHM techniques, e.g., Lamb wave based approaches [Hu, Shimo-mukai, Yan and Fukunaga (2008)], a method based on impact force identification is considered to be effective because the location and the extent of the structural damage can be predicted from the impact location and force history. Thus, impact force identification of CFRP structures is an important research topic and has been investigated by many researchers.

Investigations reported so far have dealt with impact force identification of various structures, such as composite laminated plates [Wu, Yeh and Yen (1994); Tracy and Chang (1998); Hu, Fukunaga, Matsumoto, Yan and Peng (2007); Hu, Matsumoto, Nishi and Fukunaga (2007)], sandwich panels [Tsai and Wu (1998); Minakuchi, Mizutani, Akino, Takeda, Tsutsui, Hirano, Kimoto and Koshioka (2011)] and stiff-ened panels [Zhang, Zhang, Wu and Du (2008); Sekine and Atobe (2009); Yan and Zhou (2009)]. The identification methods proposed in these works were de-veloped based on an analytical or numerical model of the structure, and therefore their accuracies are strongly dependent on the adequacy of the model. On the other hand, direct experimental identification methods which do not require any analyti-cal or numerical model of the structure are also reported. For these approaches, the relations between the impact force and the sensor responses are expressed by ex-perimental transfer matrices [Miyazawa, Sugimoto, Hu and Fukunaga (2007)] and system transfer functions [Park, Ha and Chang (2009)] which are determined using the measured data obtained from prior impact tests, and then the impact location and force history are identified by minimizing the deviation between the measured sensor responses and the estimated responses. For complex structures, it is difficult to construct the corresponding accurate analytical or numerical models, therefore the direct experimental identification methods are more practical.

In this paper, an experimental method for identifying the location and force history of an impact force acting on CFRP structures is presented. The present identifi-cation method is based on experimental transfer matrices which relate the impact force to the responses of piezoelectric sensors. In order to reduce the time required to identify an impact event, arrival times of the flexural waves from the impact lo-cation to the sensors are used for quickly identifying the impact location. As for the determination of the arrival times, the double peak method [Seydel and Chang (2001)], cross-correlation [Ohkami and Tanaka (1998)] and wavelet analysis [Sung, Oh, Kim and Hong (2000); Meo, Zumpano, Piggott and Marengo (2005); Wang, Takatsubo, Akimune and Tsuda (2005)] are well-known, which have been already used for impact location identification. In the present study, an analog band-pass filter is used for the purpose of quick and accurate determination of the arrival

times. The sensor responses firstly pass through the filter, and then the arrival times are determined from the filtered outputs. The details of the identification method are described in Section 2. In Section 3, impact forces acting on CFRP laminated plates are identified experimentally in order to verify the effectiveness of the present method. Then, the identification method is further extended to a CFRP stiffened panel in Section 4. Finally, a summary of the present study is provided in Section 5.

2 Method for identifying the impact force

2.1 Construction of experimental transfer matrices

The transfer matrix used for the impact force identification is constructed experimentally. As a preparatory work, impact tests are preliminarily conducted with an impulse hammer and the experimental transfer matrix is constructed using the measured force histories and sensor responses.

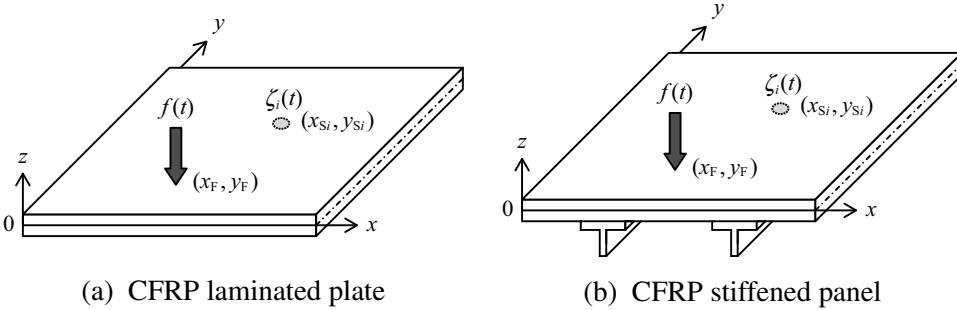(a) CFRP laminated plate   (b) CFRP stiffened panel

Figure 1: CFRP structures subjected to impact forces

Figure 1 depicts two CFRP structures subjected to impact forces, which are a laminated plate shown in Fig. 1 (a) and a stiffened panel shown in Fig. 1 (b), respectively. The stiffened panel consists of a CFRP laminated skin and two blade stiffeners. A Cartesian coordinate system (x, y, z) shown in Fig. 1 is adopted, whose $x - y$ plane coincides with the mid-plane of the laminate. The impact force acts perpendicularly on the upper surface of the structure at (x_F, y_F), and the compressive force $f(t)$ on the plates is assumed. With a total of $M (\geq 3)$ piezoelectric sensors bonded on the undersurface of the structure at (x_{Si}, y_{Si}) $(i = 1, \ldots, M)$, the corresponding responses $\zeta_i(t)$ $(i = 1, \ldots, M)$ are measured at the sampling rate of $1/\Delta t_s$. Note that the response of a disk type PZT sensor is a voltage signal which is proportional to the sum of the normal strains in the x and y axes directions. The relation between the impact force and the response of the ith sensor can be expressed in the

following equation:

$$\{\boldsymbol{\zeta}_i\} = [G(x_F, y_F, x_{Si}, y_{Si})]\{\boldsymbol{f}\} \tag{1}$$

where

$$\{\boldsymbol{\zeta}_i\} = [\zeta_i(t_1)\ \zeta_i(t_2)\ \cdots\ \zeta_i(t_N)]^T, \quad \{\boldsymbol{f}\} = [f(t_1)\ f(t_2)\ \cdots\ f(t_N)]^T,$$

$$[G(x_F, y_F, x_{Si}, y_{Si})] = \begin{bmatrix} g_1 & 0 & \cdots & 0 \\ g_2 & g_1 & \ddots & \vdots \\ \vdots & \vdots & \ddots & 0 \\ g_N & g_{N-1} & \cdots & g_1 \end{bmatrix}. \tag{2}$$

Here, $\zeta_i(t_n)$ and $f(t_n)$ are the sensor response and force measured at the time $t_n = n\Delta t_s$ $(n = 1, \ldots, N)$, respectively. $[G(x_F, y_F, x_{Si}, y_{Si})]$ is a transfer matrix composed of the Green's function. It is worthwhile to note that the transfer matrix is defined by a function of the impact location (x_F, y_F) and sensor location (x_{Si}, y_{Si}), and is not dependent on the force history.

By rewriting Eq. 1, we obtain

$$\{\boldsymbol{\zeta}_i\} = [F]\{\boldsymbol{g}\} \tag{3}$$

where

$$\{\boldsymbol{g}\} = [g_1\ g_2\ \cdots\ g_N]^T, \quad [F] = \begin{bmatrix} f(t_1) & 0 & \cdots & 0 \\ f(t_2) & f(t_1) & \ddots & \vdots \\ \vdots & \vdots & \ddots & 0 \\ f(t_N) & f(t_{N-1}) & \cdots & f(t_1) \end{bmatrix}. \tag{4}$$

The components of the transfer matrix are determined in a way where the estimated responses given by Eq. 3 using the measured force histories, are adjusted to match the measured responses as much as possible. In order to increase the reliability of the obtained transfer matrix, the experimental data are acquired by repeating impact tests of K times. Thus, the components of the transfer matrix are obtained by solving the minimization problem as follows:

$$\text{minimize} : \sum_{k=1}^{K} \left\| \{\boldsymbol{\zeta}_i^k\} - [F^k]\{\boldsymbol{g}\} \right\|^2 \tag{5}$$

design variables : $\{\boldsymbol{g}\}$

where $\{\boldsymbol{\zeta}_i^k\}$ and $[F^k]$ are the vector of measured sensor responses and the force matrix of the kth impact test, respectively. Here, the least-squares method is used
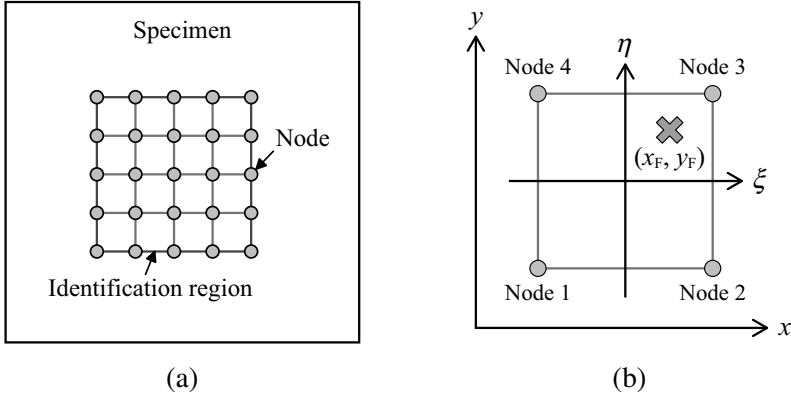
(a)   (b)

Figure 2: Interpolation of transfer matrix

to solve Eq. 5. As previously stated, the transfer matrix is defined by a function of the impact location (x_F, y_F) and sensor location (x_{Si}, y_{Si}). Therefore, to identify the impact force history, the transfer matrix is required for each sensor and for an arbitrary (x_F, y_F). Thus, the whole identification region is divided into some discrete grid areas, as shown in Fig. 2 (a), and the impact tests are conducted at every grid node. Then, the experimental transfer matrices are constructed for each set relating one node to one sensor location by employing Eq. 5. For a location inside the four nodes of each grid area, the transfer matrix is obtained by an interpolation operation using shape functions similar to those used in finite element analyses. When a four-node two-dimensional element is used, as depicted in Fig. 2 (b), the interpolation of transfer matrix is expressed as:

$$\left[G(x_F, y_F, x_{Si}, y_{Si}) \right] = \sum_{l=1}^{4} N_l \left[G(x_l, y_l, x_{Si}, y_{Si}) \right] \tag{6}$$

where

$$N_1 = \frac{1}{4}(1 - \xi_F)(1 - \eta_F), \qquad N_2 = \frac{1}{4}(1 + \xi_F)(1 - \eta_F),$$

$$N_3 = \frac{1}{4}(1 + \xi_F)(1 + \eta_F), \qquad N_4 = \frac{1}{4}(1 - \xi_F)(1 + \eta_F). \tag{7}$$

Here, (x_l, y_l) are the coordinates of node l, and (ξ_F, η_F) is the local coordinates of the impact location.

2.2 Identification method for CFRP laminated plates

Firstly, the impact location is identified using the arrival times of the flexural waves from the impact location to the PZT sensors. Figure 3 depicts the method for impact
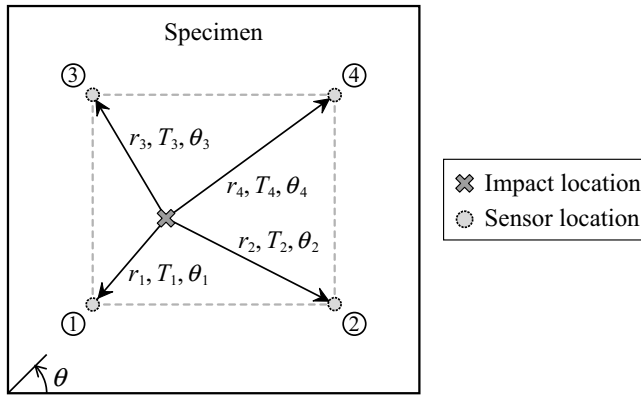
Figure 3: Schematic of impact location identification using arrival times of flexural waves

location identification. In the figure, r_i is the distance between the impact location and the sensor, T_i and θ_i are the arrival time and the propagation direction of the flexural wave, respectively, and the subscript i denotes the sensor number. Here, the $0°$ propagation direction is parallel to the x axis. The difference in the arrival times for the ith and jth sensors is given by

$$\Delta T_{ij} = T_j - T_i = \frac{r_j}{v(\theta_j)} - \frac{r_i}{v(\theta_i)} \tag{8}$$

where $v(\theta)$ is the velocity of the flexural wave propagation in the direction of an angle θ. Due to the anisotropy of the CFRP laminated plate, the wave velocity depends on the angle of propagation direction.

The impact location is identified by minimizing the deviation between the differences in the arrival times given by Eq. 8 and the differences calculated from the measured arrival times. Thus, it is formulated as:

$$\text{minimize}: \sum_{i=1}^{M-1} \sum_{j=i+1}^{M} \left[\Delta T_{ij}^* - \left\{ \frac{r_j}{v(\theta_j)} - \frac{r_i}{v(\theta_i)} \right\} \right]^2 \tag{9}$$

design variables :x_F, y_F

where ΔT_{ij}^* is those calculated from the measured arrival times, and M is the number of PZT sensors and $M = 4$ in the present study. In order to solve the minimization problem of Eq. 9, the conjugate gradient method with the golden section search method is used.

The wave velocity used to identify the impact location (i.e. $v(\theta)$ in Eq. 9) is also determined experimentally, and the details will be described in section *3.2*. As
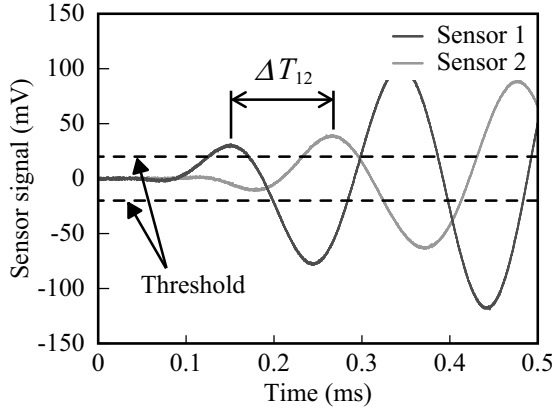
Figure 4: Detection of the arrival times of flexural waves

to the arrival times of the flexural waves, they are determined from the sensor responses filtered by a band-pass filter. By using the high-frequency components that are obtained from an analog filter with a narrow passband, the arrival times can be detected accurately and rapidly. Figure 4 shows an example of the filtered responses. In the present study, the arrival time is defined as the time of the first peak which crosses over the threshold. The threshold was set up by considering the impact test results and the magnitude of the noise in the measured data.

After the impact location is identified, with the pre-constructed experimental transfer matrices, the force history is identified by minimizing the deviation between the measured sensor responses and the responses estimated from Eq. 1. Then, the identification problem can be expressed in the following optimization problem:

$$\text{minimize}: \sum_{i=1}^{M} \left\| \{\boldsymbol{\zeta}_i\} - [G(x_\text{F}, y_\text{F}, x_{\text{S}i}, y_{\text{S}i})]\{\boldsymbol{f}\} \right\|^2$$

$$\text{subject to}: f(t) \geq 0 \tag{10}$$

$$\text{design variables}: \{\boldsymbol{f}\}$$

Here, the quadratic programming method is used to solve Eq. 10.

2.3 Identification method for CFRP stiffened panels

The identification method for stiffened panels is also based on the experimental transfer matrices, but it differs from the previous one for laminated plates. Due to the complexity of the panel, it is difficult to identify the impact location accurately using only the arrival times of the flexural waves. Therefore, an iterative method is used, and the impact location and force history are identified in parallel.

The arrival times of the flexural waves are used to determine the approximate impact location which is initially required in the iterative process. Here the method is similar to that used for laminated plates. In the case of stiffened panels, the structural properties vary with respect to location, due to the bonded stiffeners. Thus, the whole identification region is divided into two areas (i.e. skin area and stiffener area) depending on whether a stiffener is bonded on the other side, and the velocity of the flexural wave is determined independently. Then, the arrival time of the flexural wave to the ith sensor can be expressed as:

$$T_i = \frac{r_i^{\text{sk}}}{v^{\text{sk}}(\theta_i)} + \frac{r_i^{\text{st}}}{v^{\text{st}}(\theta_i)} \tag{11}$$

where the superscripts "sk" and "st" denote the skin area and the stiffener area, respectively. By employing Eq. 11, the impact location is approximately estimated by solving the following problem.

$$\text{minimize} : \sum_{i=1}^{M-1} \sum_{j=i+1}^{M} \left\{ \Delta T_{ij} - (T_j - T_i) \right\}^2 \tag{12}$$

design variables : $x_{\text{F}}, y_{\text{F}}$

Like the previous laminated plates, the number of sensors is $M = 4$, and the wave velocities $v^{\text{sk}}(\theta)$ and $v^{\text{st}}(\theta)$ in Eq. 11 are determined experimentally. In order to solve Eq. 12, the identification region is divided into a grid and the value of the objective function is calculated at every grid point. The location of the grid point of the minimum value (Eq. 12) is determined as the approximate location. In the present study, the grid spacing is set to be 0.1 mm.

Next, the equation used for identifying the accurate impact location is described. When we assume the impact location as $(x_{\text{e}}, y_{\text{e}})$, an estimated force history $\{f_{\text{e}}\}$ can be obtained by employing Eq. 10. Then, the accurate impact location which minimizes the deviation between the measured responses and the responses calculated from the estimated force history can be obtained from the following minimization problem.

$$\text{minimize} : \sum_{i=1}^{M} \left\| \{\boldsymbol{\zeta}_i\} - \left[G(x_{\text{F}}, y_{\text{F}}, x_{\text{S}i}, y_{\text{S}i}) \right] \{f_{\text{e}}\} \right\|^2 \tag{13}$$

design variables : $x_{\text{F}}, y_{\text{F}}$

Here, Eq. 13 is solved using the conjugate gradient method with the golden section search method.

The location and force history of the impact force are identified by following the procedures shown in Fig. 5. As first, the approximate impact location is estimated
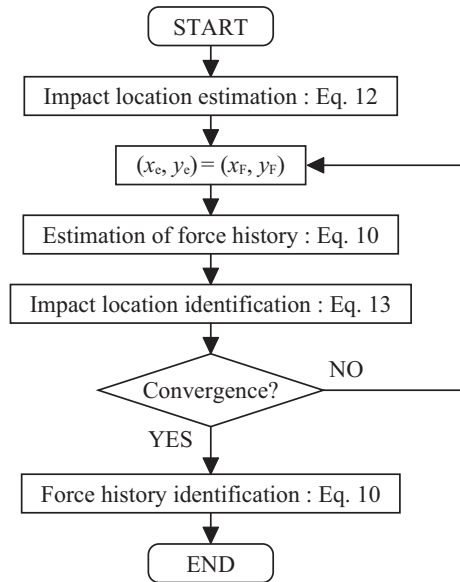
Figure 5: Flow chart of impact force identification of CFRP stiffened panels

from the arrival times by employing Eq. 12, and this location is used as the initial (x_e, y_e). After the estimated force history is obtained, the impact location is updated from Eq. 13. The same process is repeated until the impact location converges to a certain point. Finally, the force history is identified from Eq. 10.

3 Impact force Identification of CFRP laminated plates

3.1 Experimental setup

Figure 6 shows the square CFRP laminated plate used in this study. The side length of the plate is 300 mm and the thickness is 2 mm. Two plates with different laminate sequences: $[0_2/45_2/-45_2/90_2]_s$ (CFRP1) and $[45_2/-45_4/45_2]_s$ (CFRP2) are used in the experiment. Here, the thickness of a CFRP lamina is 0.25 mm and the $0°$ direction of the fiber orientation is parallel to the x axis. Four disk-type PZT sensors (Fuji Ceramics C-64) of the diameter of 4 mm and the thickness of 0.3 mm, are bonded on the bottom surface of the plate. The sensor locations are $(90, 90)$, $(210, 90)$, $(90, 210)$ and $(210, 210)$ in mm. As shown in Fig. 6, the plate is clamped at the four corners.

The schematic of the experimental setup is shown in Fig. 7. An impact force is applied to the specimen using an impulse hammer (Dytran Instruments 5850B) powered by a power unit (Dytran Instruments 4102C). The signals from the PZT sen-
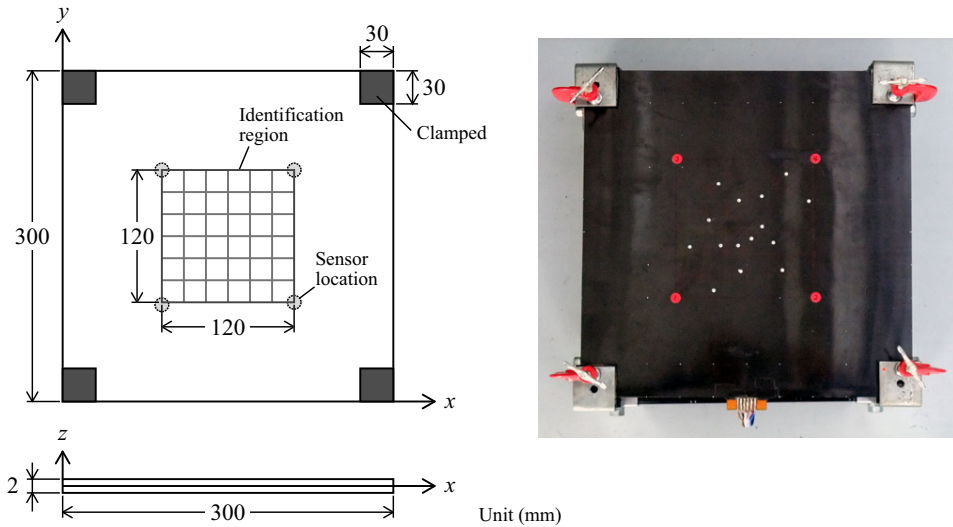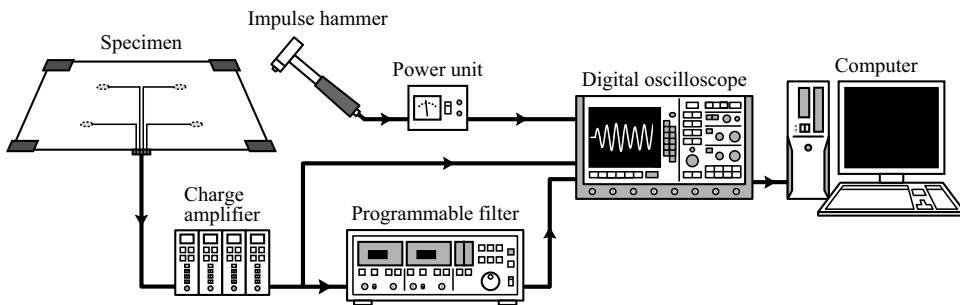
Figure 6: CFRP laminated plate

Figure 7: Experimental setup

sors are amplified by a charge amplifier (Ono Sokki CH1200) and then measured with a digital oscilloscope (Keyence GR-7000). In addition, the sensor responses are transmitted to a programmable filter (NF 3627) and the filtered sensor signals are measured simultaneously. Moreover, the force of the impulse hammer is also directly measured. By using these measured data, the impact force identification is performed by a computer.

In the present experiment, an impact tip made of hard plastic is attached to the impulse hammer. The sensor signals and force responses, which are used in the force history identification, are measured in the time period of 14 ms and the sampling time is set as $\Delta t_s = 40\,\mu$s. As to the filtered responses which are used to identify the impact location, the time period and sampling time are set to be 1 ms and $0.1\,\mu$s, respectively.

3.2 *Experimental transfer matrices and wave velocity*

As shown in Fig. 6, the identification region of the impact force is a square region with one side 120 mm in length, i.e. $90 \leq x_F, y_F \leq 210$. The identification region is equally divided into six sections in the directions of the x and y axes, and the experimental transfer matrices are determined at the 49 grid nodes. The number of impact tests conducted for each node is $K = 5$.

Like the transfer matrices used to identify the force history, the wave velocity $v(\theta)$ used for impact location identification is also determined experimentally from impact test results. Figure 8 depicts the impact test conducted in order to determine the wave velocity. The impact location and the PZT sensors are located on a line, and the difference in the arrival times, ΔT_{ij}, and the distance between the two sensors, Δr_{ij}, are measured. Impact tests are conducted five times for each pair of

$$\Delta r_{ij} = v(\theta) \Delta T_{ij}$$
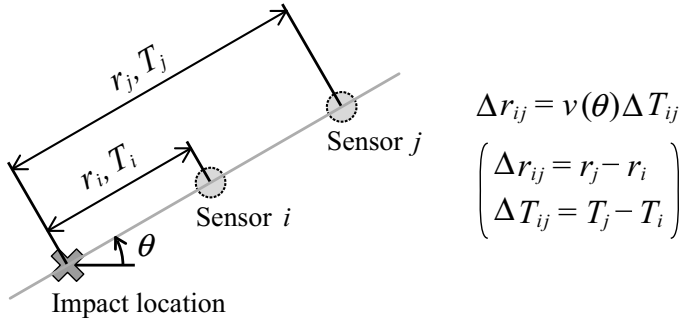$$\begin{pmatrix} \Delta r_{ij} = r_j - r_i \\ \Delta T_{ij} = T_j - T_i \end{pmatrix}$$

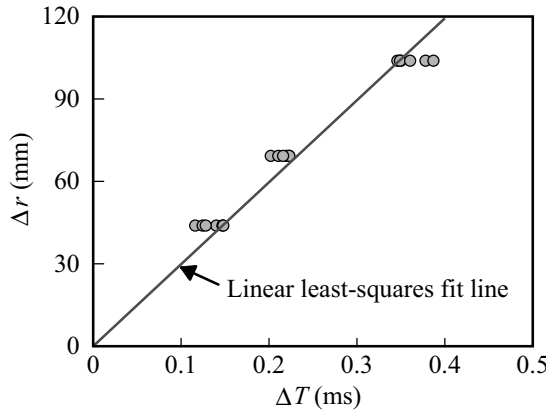Figure 8: Impact test for determining the wave velocity

Figure 9: Δr versus ΔT (CFRP1, $\theta = 90°$)

sensors and the wave velocity is determined using the least-squares method. Since the wave velocity is dependent on propagation direction, the velocity is determined at multiple angles. Thus, in addition to the four PZT sensors that are used for identifying the impact force, six more sensors are used in determining the wave velocity. Note that the center frequency of the band-pass filter and the threshold, which are used to detect the arrival times of the flexural wave, are also determined on the basis of these impact test results by considering the amplitude of the filtered response and the magnitude of the noise.

As an example, Fig. 9 shows the relation between ΔT and Δr of a flexural wave propagating through CFRP1 at an angle of 90 degrees. Here, the center frequency of the band-pass filter is set as $f_c = 5\,\mathrm{kHz}$, and the impact tests are conducted for three pairs of sensors of different intervals. The wave velocity is determined from the slope of the linear least-squares fitted line.
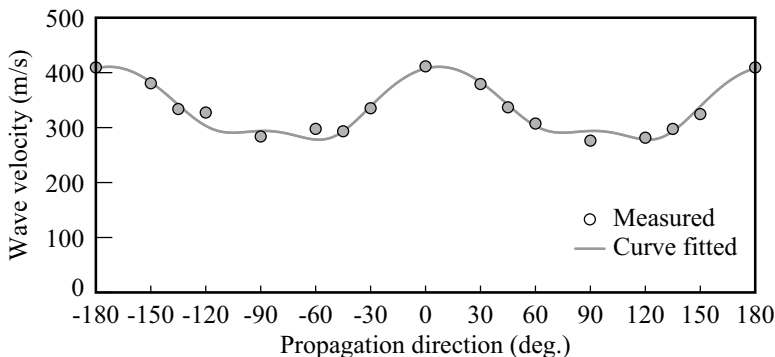
(a) CFRP1 : $[0_2/45_2/-45_2/90_2]_s$
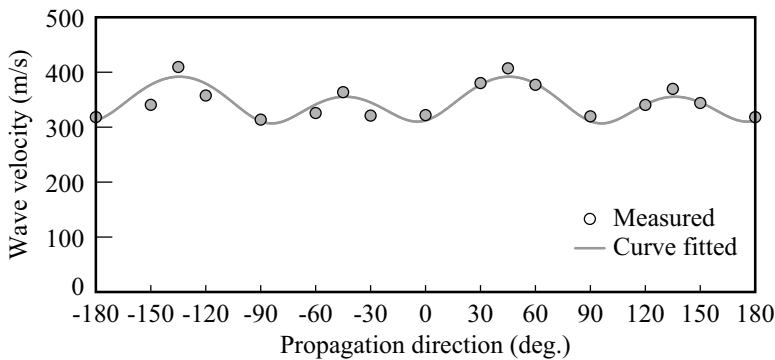
(b) CFRP2 : $[45_2/-45_4/45_2]_s$

Figure 10: Propagation direction dependence of wave velocity (CFRP laminated plate)

Figure 10 shows the propagation direction dependence of the wave velocity for the two CFRP laminated plates. In the figure, the mark $\bigcirc$ denotes the wave velocity determined from the measured data, and the solid line is a fitted curve. In order to obtain a continuous function $v(\theta)$, a curve fitting was performed by employing the following equation which gives the phase velocity for an orthotropic plate [Doyle (1997)]:

$$v(\theta) = \sqrt[4]{\omega^2 \frac{D_{\theta\theta}}{\rho h}} \tag{14}$$

where

$$\begin{aligned} D_{\theta\theta} = {} & D_{11} \cos^4\theta + 2(D_{12} + 2D_{66}) \cos^2\theta \sin^2\theta + D_{22} \sin^4\theta \\ & + 4D_{16} \cos^3\theta \sin\theta + 4D_{26} \cos\theta \sin^3\theta \ . \end{aligned} \tag{15}$$

Here, ρ, h, D_{mn} ($m = 1, 2, 6$; $n = 1, 2, 6$) are the density, thickness and bending stiffness of the CFRP laminated plate, respectively, and ω ($= 2\pi f_c$) is the angular frequency of the flexural wave. The coefficients of the circular functions in Eq. 15 are determined from the measured wave velocities by performing a least-squares fitting. In the impact location identification, the fitted curve is used as $v(\theta)$.

3.3 Identification results and discussion

The results of impact location identification are shown in Fig. 11. In the figure, the marks $\bigodot$ and $\bigotimes$ denote the identified location of the impact force and the measured location, respectively. The identification was performed at 12 points for each plate, and the locations were identified within the error of 6.6 mm in the case of CFRP1, and 8.4 mm for CFRP2. Here, the error of impact location identification is defined as the distance between the identified location and the measured one. Points A and B depicted in Fig. 11 correspond to the point of each plate where the error of impact location identification was the maximum.

Figure 12 shows the identification results of force history for points A, B, C and D depicted in Fig. 11. In this figure, dashed lines denote the identified force histories and solid lines the measured ones. As can be seen from the figure, even though the force history is rough since the contact between the plate and the impactor occurs multiple times, the identified force histories are in good agreement with the measured ones.

In order to evaluate the identification accuracy of force history, the error of the identified force is defined as follows:

$$E_F = \frac{\left| f_m(t_{p_m}) - f_{id}(t_{p_m}) \right|}{\left| f_m(t_{p_m}) \right|} \tag{16}$$
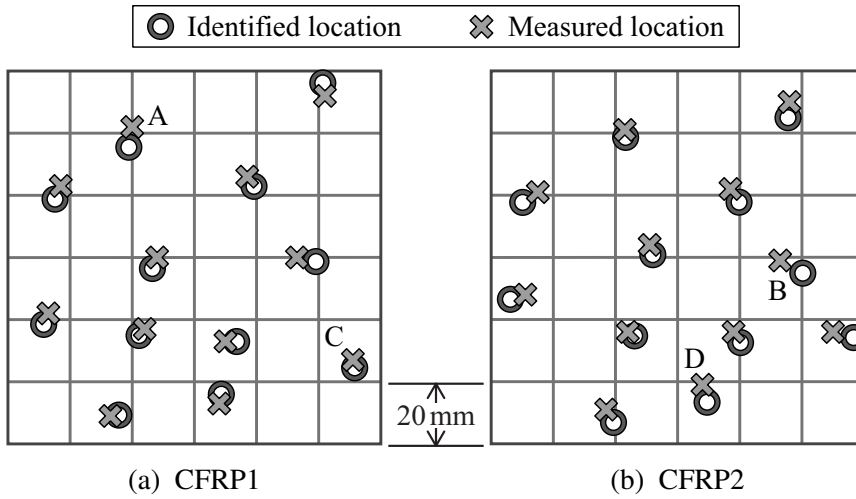
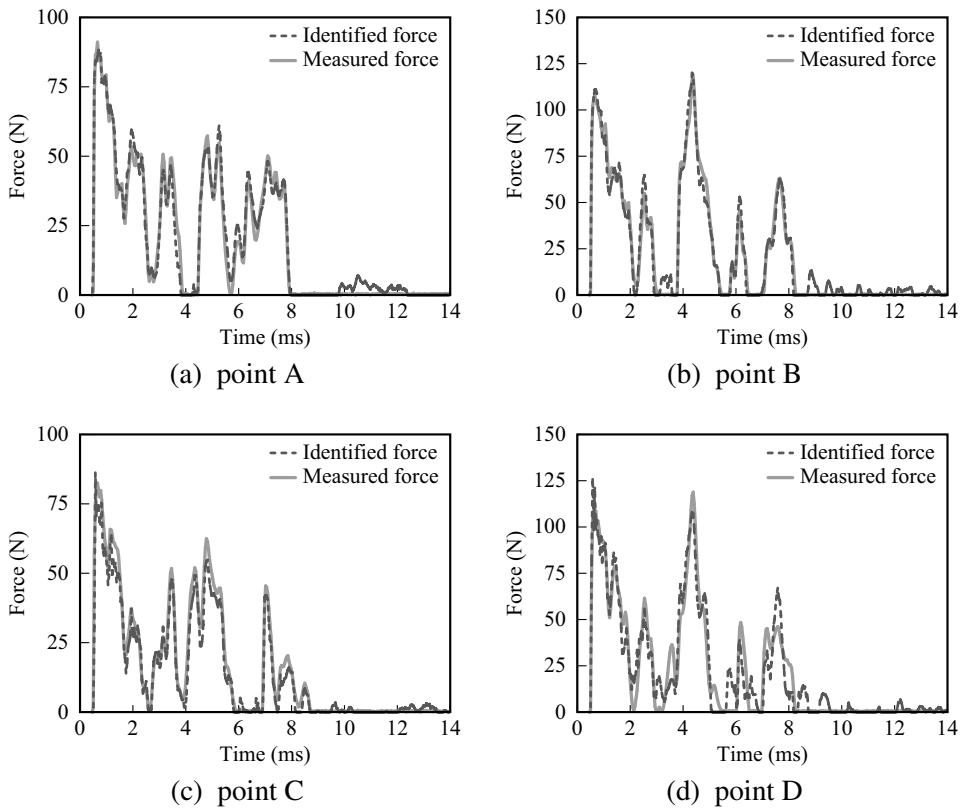Figure 11: Identification results of impact location (CFRP laminated plate)

Figure 12: Identification results of force history (CFRP laminated plate)

where $f_m(t)$ and $f_{id}(t)$ are the measured and identified forces, respectively, and t_{p_m} is the time of the peak of the measured force. The errors of the identified forces for points A and B were 5.48% and 0.07%, respectively. The maximum errors of force history identification for CFRP1 and CFRP2 were 10.0% (point C) and 9.60% (point D), respectively. The results reveal that regardless of the laminate sequence, the impact location is identified with sufficient accuracy using the arrival times of the flexural waves and the wave velocity determined experimentally. Moreover, it is revealed that the force history can also be identified accurately using the experimental transfer matrices.

Furthermore, the validity of the present method is verified by comparing the identification results with those in our previous work based on an optimization technique [Miyazawa, Sugimoto, Hu and Fukunaga (2007)]. In our previous work, the initial impact location is estimated using all nodes shown in Fig. 6 by performing a parametric calculation. Figure 13 shows the comparison results of the identification errors. In the figure, the bars show the average of the error and the vertical lines indicate the range. Although there is a slight difference in the accuracy of impact location identification between the two methods, there is not much difference in the accuracy of the identified forces. Thus, it can be considered that the two methods are equivalent in accuracy.

Next we compare the identification times for both methods as shown in Fig. 14. The present method can be considered as real-time identification since the time required to identify an impact force is approximately only 1 second. On the other hand, the method based on an optimization technique requires more than 15 seconds. The present method is capable of identifying the impact force in real time
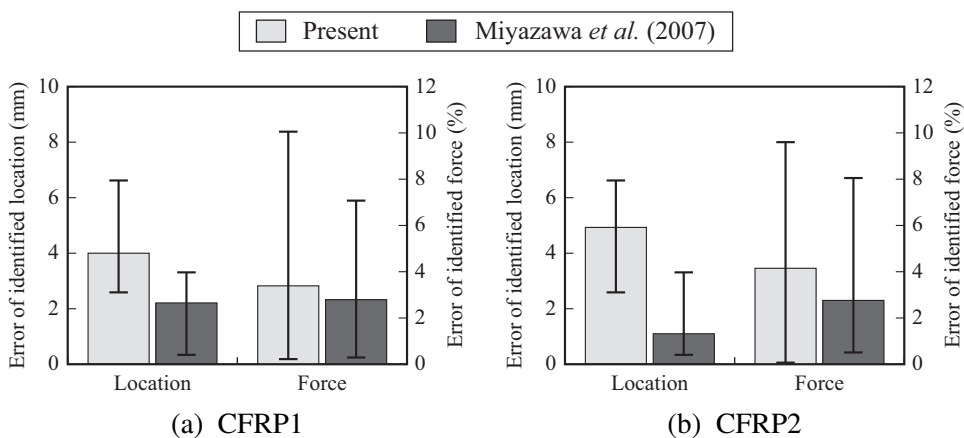

Figure 13: Comparison of identification errors (CFRP laminated plate)

because the impact location and the force history are identified separately, which is achieved by identifying the impact location from the arrival times of the flexural waves. In addition, instead of using a time consuming (computationally expensive) method, such as cross-correlation and wavelet analysis which are generally used to detect the arrival times, the use of a band-pass filter also led to the reduction of the identification time.
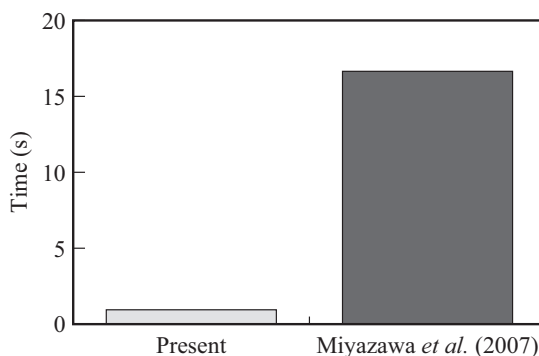

Figure 14: Comparison of time required for identification (CFRP laminated plate)

4   Impact force identification of CFRP stiffened panels

4.1   Experimental setup

Figure 15 shows the specimen of the CFRP stiffened panel. The laminate sequence of the panel is shown in Tab. 1, where the fiber direction of $0°$ is parallel to the y axis. As shown in Fig. 15, the two edges perpendicular to the stiffeners are clamped by jigs. Six PZT sensors, which are identical with those used for the CFRP laminated plates, are bonded on the bottom surface of the panel at the locations indicated in Tab. 2. The experimental system is also identical with that depicted in Fig. 7. The responses of PZT sensors and the force are measured in the time period of 5 ms and the sampling rate is set as $\Delta t_{\mathrm{s}} = 20\,\mu\mathrm{s}$. The center frequency of the band-pass filter is set as $f_{\mathrm{c}} = 10\,\mathrm{kHz}$, and the filtered responses are measured for 1 ms at intervals of $0.1\,\mu\mathrm{s}$.

The identification region is a rectangular region of 120 mm in length $(90 \leq y \leq 210)$ and 150 mm in width $(10 \leq x \leq 160)$. Figure 16 shows the mesh for constructing the experimental transfer matrices. In the figure, the stiffener area is shaded for the purpose of distinction. It is worthwhile to note that the intervals in the direction of the x axis are determined by considering the locations where the structural properties
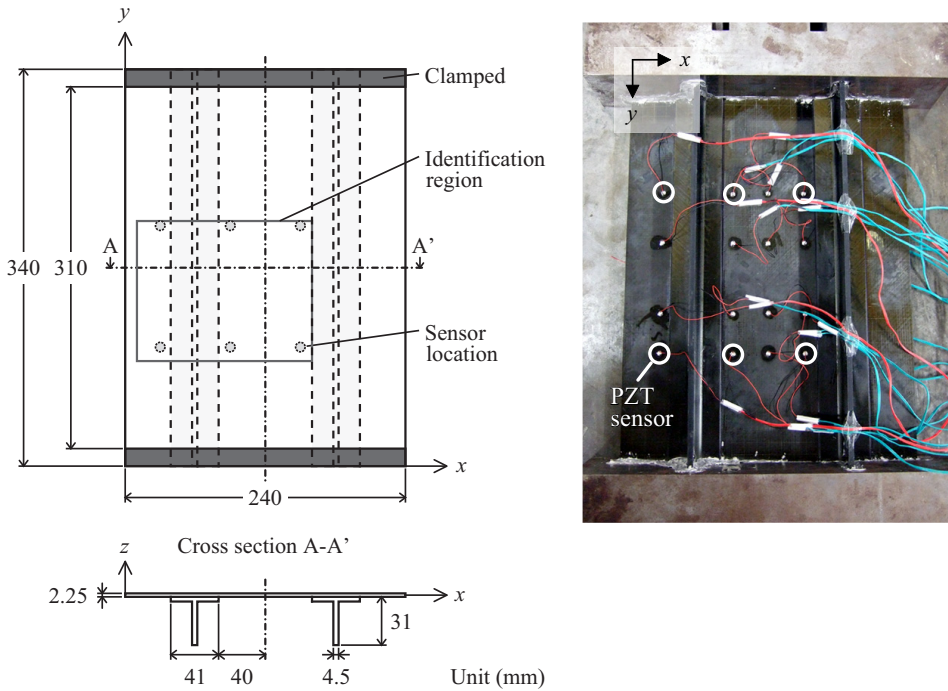
Figure 15: CFRP stiffened panel

Table 1: Laminate sequence of CFRP stiffened panel

Skin	$\left[-45\,/\,0\,/\,45\,/\,90_2\,/-45\,/\,0\,/\,45\,/\,90\right]_s$
Flange	$\left[(-45\,/\,90\,/\,45\,/\,0\,/-45\,/\,90_2\,/\,45\,/\,90)_s\,/\,(-45\,/\,90\,/\,45)_s\right]$
Web	$\left[(-45\,/\,90\,/\,45\,/\,0\,/-45\,/\,90_2\,/\,45\,/\,90)_s\right]_s$

Table 2: Sensor locations (CFRP stiffened panel)

Sensor 1	Sensor 2	Sensor 3	Sensor 4	Sensor 5	Sensor 6
(30,102)	(90,102)	(150,102)	(30, 206)	(90, 206)	(150, 206)

suddenly change, such as the locations of the edges of the flange and the location of the web. The number of nodes is 70 and the number of impact tests conducted for each node is $K=5$. In Fig. 16, the circled numbers indicate the sensor numbers and the dashed line denoted by B is a borderline that separates the identification region

Figure 16: Mesh for constructing experimental transfer matrices

according to the sensors that are used in the identification. Sensors 1, 2, 4 and 5 are used in the left region and sensors 2, 3, 5 and 6 are used in the right.

4.2   Identification results and discussion

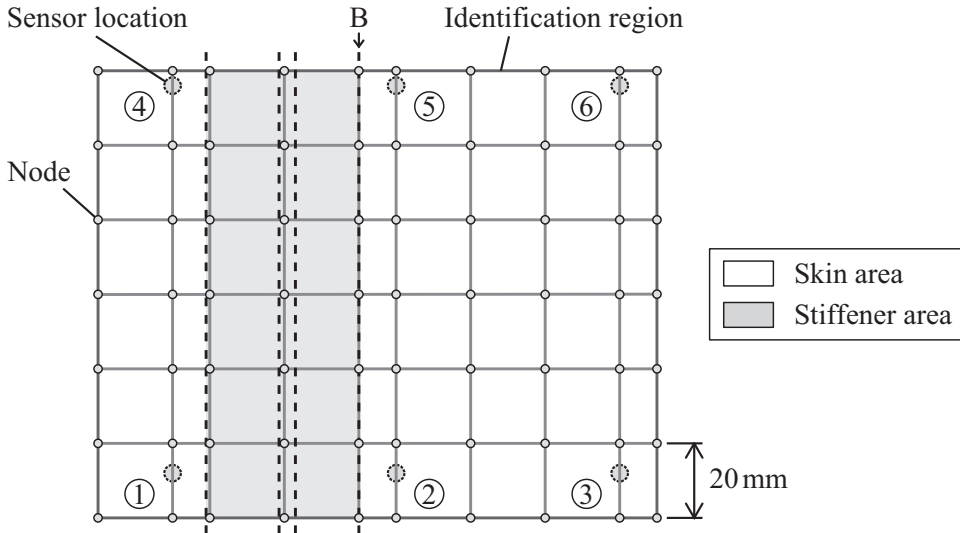Figure 17 shows the impact location determined from the arrival times of the flexural waves. In the figure, the marks ◎ and ✖ denote the estimated and measured locations, respectively. The estimation is performed at 33 points and the corresponding pairs are enclosed by ellipses. As can be seen from the figure, the estimated locations deviate from the measured locations at many points. The average error of the estimated locations was 15.5 mm, and the maximum error was 45.3 mm. In the case of stiffened panels, it is more difficult to detect the accurate arrival times compared to laminated plates, because the flexural waves are affected by the stiffeners. Therefore, an identification method based on an optimization technique is considered to be more effective in the case of complex structures.

The identification results of impact location are shown in Fig. 18. Compared to the results of impact location estimation (Fig. 17), we can see that the identified locations show excellent agreement with the measured locations. The locations were identified within the error of 11.8 mm. In this case, it took approximately 4 seconds to identify an impact force. The results of force history identification for points A, B, C and D are shown in Fig. 19, and the identification errors of each point are indicated in Tab. 3. The figure and the table reveal that the impact location and force history are both identified accurately at every point. The maximum error
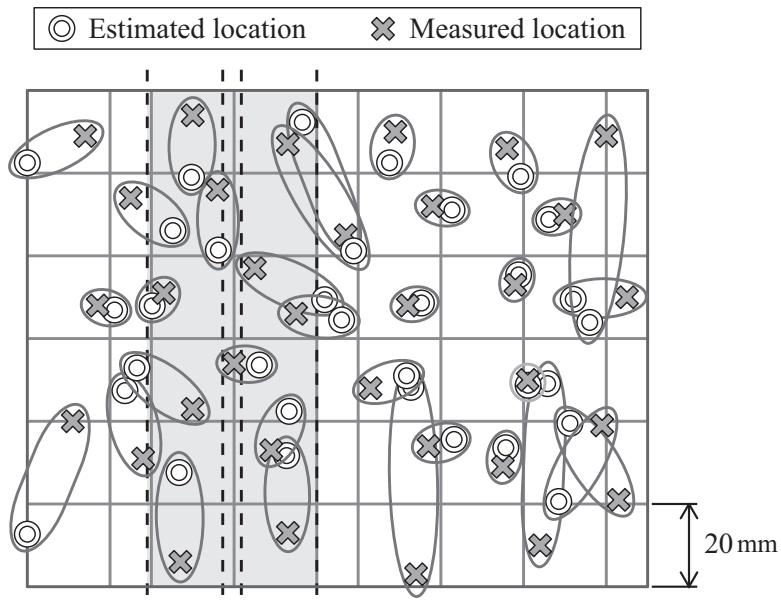
Figure 17: Results of impact location estimation
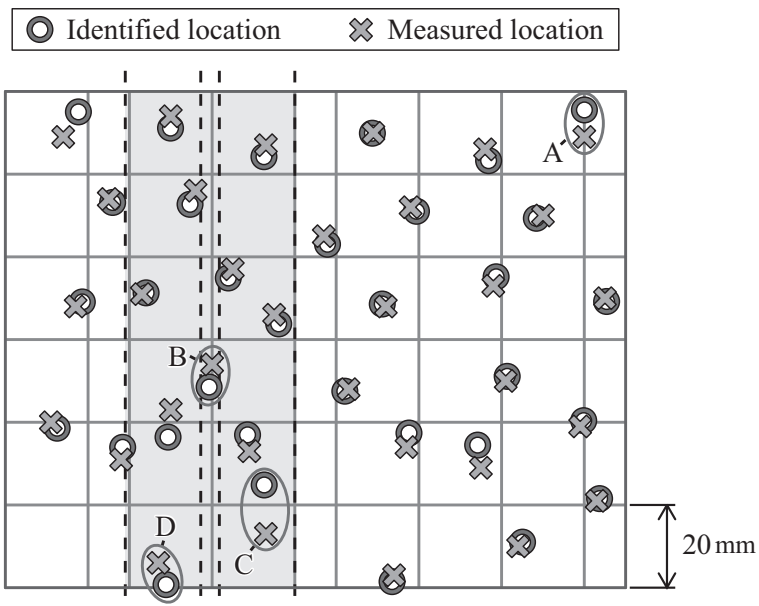
Figure 18: Identification results of impact location (CFRP stiffened panel)

of the identified force histories was 13.6%.

(a) point A   (b) point B
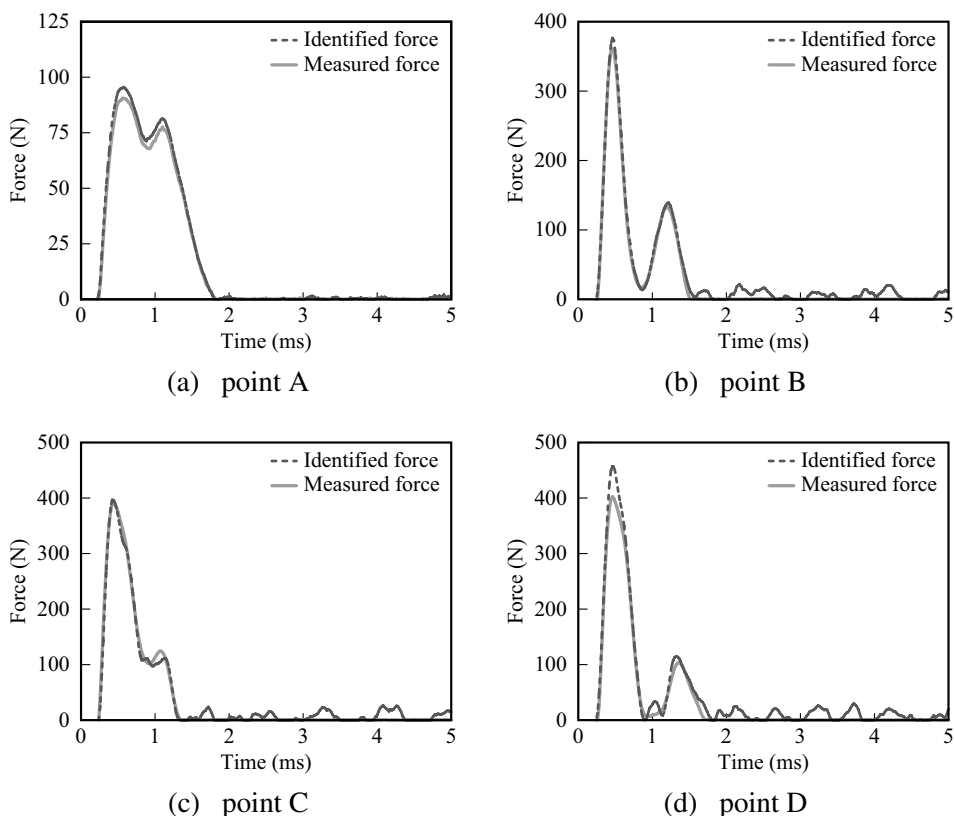
(c) point C   (d) point D

Figure 19: Identification results of force history (CFRP stiffened panel)

Table 3: Identification errors of points A, B, C and D

	Point A	Point B	Point C	Point D
Error of identified location	6.5 mm	5.5 mm	11.8 mm	5.6 mm
Error of identified force	5.0%	4.3%	1.5%	13.6%

Figure 20 shows the plot of the error of the identified force versus the error of the location. In the figure, the marks ◇ and ◉ denote the results for impact forces acting on the skin area and the stiffener area, respectively. As can be seen from the figure, there is no big difference in accuracies of impact force identification

Figure 20: Error of identified force versus error of identified location

between the two areas. Moreover, it can be said that there is a positive correlation between the impact location error and the force history error.

5 Conclusions

In this paper, a method for identifying the location and force history of an impact force acting on a CFRP structure has been developed by using the experimental transfer matrices that relate the impact force to the corresponding sensor responses. In the impact location identification, the arrival times of the flexural waves to the sensors are used in order to reduce the identification time. The validity of the proposed method has been verified experimentally through identification of impact forces acting on CFRP laminated plates. Then, the identification method was applied to a CFRP stiffened panel. The knowledge obtained from the results is summarized as follows:

- The method proposed for CFRP laminated plates is capable of identifying the location and force history accurately and in real time. The identification results reveal that, owing to the experimentally determined transfer matrices and wave velocity, the accuracy of identification is not dependent on the laminate sequence. Moreover, it has been found, through comparison with a different identification method, that the use of arrival times of the flexural waves for identifying the impact location is effective in reducing the identification time.

- The results reveal that the identification method based on the experimental

transfer matrices is capable of identifying impact forces acting on complex structures such as CFRP stiffened panels. The impact location is identified accurately by determining the initial location from the arrival times of the flexural waves and then updating the location using an optimization method. The force history is also identified with sufficient accuracy by using the experimental transfer matrices. It has been found that the present method can identify an impact force within a few seconds.

References

Doyle, J. F. (1997): *Wave Propagation in Structures, Second Edition*. Springer.

Hu, N. (1997): A solution method for dynamic contact problems. *Comput. & Struct.*, vol. 63, no. 6, pp. 1053–1063.

Hu, N.; Fukunaga, H.; Matsumoto, S.; Yan, B.; Peng, X. H. (2007): An efficient approach for identifying impact force using embedded piezoelectric sensors. *Int. J. Impact Engng.*, vol. 34, no. 7, pp. 1258–1271.

Hu, N.; Matsumoto, S.; Nishi, R.; Fukunaga, H. (2007): Identification of impact forces on composite structures using an inverse approach. *Struct. Eng. Mech.*, vol. 27, no. 4, pp. 409–424.

Hu, N.; Sekine, H.; Fukunaga, H.; Yao, Z. H. (1999): Impact analysis of composite laminates with multiple delaminations. *Int. J. Impact Engng.*, vol. 22, no. 6, pp. 633–648.

Hu, N.; Shimomukai, T.; Yan, C.; Fukunaga, H. (2008): Identification of delamination position in cross-ply laminated composite beams using S_0 Lamb mode. *Compos. Sci. Tech.*, vol. 68, no. 6, pp. 1548–1554.

Hu, N.; Zemba, Y.; Okabe, T.; Yan, C.; Fukunaga, H.; Elmarakbi, A. M. (2008): A new cohesive model for simulating delamination propagation in composite laminates under transverse loads. *Mech. Mater.*, vol. 40, no. 11, pp. 920–935.

Li, C. F.; Hu, N.; Cheng, J. G.; Fukunaga, H.; Sekine, H. (2002): Low-velocity impact-induced damage of continuous fiber-reinforced composite laminates, Part II. Verification and numerical investigation. *Compos. Part A*, vol. 33, no. 8, pp. 1063–1072.

Li, C. F.; Hu, N.; Yin, Y. J.; Sekine, H.; Fukunaga, H. (2002): Low-velocity impact-induced damage of continuous fiber-reinforced composite laminates, Part I. An FEM numerical model. *Compos. Part A*, vol. 33, no. 8, pp. 1055–1062.

Meo, M.; Zumpano, G.; Piggott, M.; Marengo, G. (2005): Impact identification on a sandwich plate from wave propagation responses. *Compos. Struct.*, vol. 71, no. 3-4, pp. 302–306.

Minakuchi, S.; Mizutani, T.; Akino, N.; Takeda, N.; Tsutsui, H.; Hirano, N.; Kimoto, J.; Koshioka, Y. (2011): Impact identification for CFRP foam-core sandwich structures using dynamic strain measurement by multiplexed FBG sensor. *J. Jpn. Soc. Aeronaut. Space Sci.*, vol. 59, no. 691, pp. 212–221. (in Japanese).

Miyazawa, H.; Sugimoto, S.; Hu, N.; Fukunaga, H. (2007): Experimental identification of impact force location and history on CFRP composite structures. *J. Jpn. Soc. Compos. Mater.*, vol. 33, no. 3, pp. 87–94. (in Japanese).

Ohkami, Y.; Tanaka, H. (1998): Estimation of the force and location of an impact exerted on a spacecraft. *JSME Int. J. Series C*, vol. 41, no. 4, pp. 829–835.

Park, J.; Ha, S.; Chang, F. K. (2009): Monitoring impact events using a system-identification method. *AIAA J.*, vol. 47, no. 9, pp. 2011–2021.

Sekine, H.; Atobe, S. (2009): Identification of locations and force histories of multiple point impacts on composite isogrid-stiffened panels. *Compos. Struct.*, vol. 89, no. 1, pp. 1–7.

Sekine, H.; Hu, N. (1998): Low-velocity impact response of composite laminates with a delamination. *Mech. Compos. Mater. & Struct.*, vol. 5, no. 3, pp. 257–278.

Seydel, R.; Chang, F. K. (2001): Impact identification of stiffened composite panels, I. System development; II. Implementation studies. *Smart Mater. Struct.*, vol. 10, no. 2, pp. 354–369; 370–379.

Staszewski, W. J.; Boller, C.; Tomlinson, G. R. (2004): *Health Monitoring of Aerospace Structures*. John Wiley & Sons.

Sung, D. U.; Oh, J. H.; Kim, C. G.; Hong, C. S. (2000): Impact monitoring of smart composite laminates using neural network and wavelet analysis. *J. Intell. Mater. Syst. Struct.*, vol. 11, no. 3, pp. 180–190.

Tracy, M.; Chang, F. K. (1998): Identifying impacts in composite plates with piezoelectric strain sensors, Part I: Theory; Part II: Experiment. *J. Intell. Mater. Syst. Struct.*, vol. 9, no. 11, pp. 920–928; 929–937.

Tsai, C. Z.; Wu, E. (1998): Forward and inverse analysis for impact on sandwich panels. *AIAA J.*, vol. 36, no. 11, pp. 2130–2136.

Wang, B.; Takatsubo, J.; Akimune, Y.; Tsuda, H. (2005): Development of a remote impact damage identification system. *Struct. Control Health Monit.*, vol. 12, no. 3-4, pp. 301–314.

Wu, E.; Yeh, E. B.; Yen, C. S. (1994): Impact on composite laminated plates: An inverse method. *Int. J. Impact Engng.*, vol. 15, no. 4, pp. 417–433.

Yan, G.; Zhou, L. (2009): Impact load identification of composite structure using genetic algorithms. *J. Sound Vib.*, vol. 319, no. 3-5, pp. 869–884.

Zhang, B.; Zhang, J.; Wu, Z.; Du, S. (2008):   A load reconstruction model for advanced grid-stiffened composite plates. *Compos. Struct.*, vol. 82, no. 4, pp. 600–608.